DOI: 10.1002/ejic.200800473

IR Laser-Induced Carbothermal Reduction of Silica

Markéta Urbanová,[a] Dana Pokorná,[a] Snejana Bakardjieva,[b] Jan Šubrt,[b] Zdeněk Bastl,[c] and Josef Pola*[a]

Keywords: IR laser / Carbothermal reduction / Silica / Carbon–silicon oxycarbide / Nanocomposite

Pulsed IR-laser irradiation of silica in the presence of gaseous hydrocarbons (benzene or ethyne) results in carbothermal reduction of silica by hydrocarbon decomposition products and allows deposition of amorphous solids which were analyzed by FTIR, Raman, X-ray photoelectron and Auger spectra and by electron microscopy and revealed as nanosized carbon–silicon oxycarbide composites containing crystalline silica domains. The reported IR laser-induced process is the first approach to deposition of nanosized carbon–silicon oxycarbide composites.

Introduction

Carbon and silica composites are of increasing importance due to their properties (high electrical conductivity, intercalating capability, high-thermal stability, and corrosion resistance), industrial use as precursors for silicon carbide ceramic[1] and reinforcing components to so-called "green" tires,[2] as well as promising applications as low-cost solar absorbers[3,4] and novel catalytic systems.[5]

Nanosized forms of carbon–silica composites and of silicon oxycarbide have received a great deal of attention recently. The former are important for providing intimate contact between and homogeneous distribution of both constituents, which is a prerequisite for high yield of carbothermal reduction[6,7] of silica by carbon to silicon carbide.[1]

The nanostructured composites of carbon and silica were prepared by carbonization inside silica pores,[3] using sol–gel synthesis of silica–carbon precursor composites,[4,8] intercalation and hydrolysis of alkoxysilane in graphite oxide[9,10] and similar mechanochemical approaches,[11] addition of carbon precursor to silica sol solution,[12,13] monomer polymerization during the sol–gel process,[14] thermal decomposition of silicon grease[15] and carbonization of phenylene–silica hybrids.[16] Other methods involve coating fumed silica particles with carbon from pyrolysis of hydrocarbon gas,[1] flame synthesis from ethyne and silicon tetrachloride,[17] and combustion of hexamethyldisiloxane.[18,19]

[a] Laboratory of Laser Chemistry, Institute of Chemical Process Fundamentals, Academy of Sciences of the Czech Republic, 16502 Prague, Czech Republic
Email: pola@icpf.cas.cz
[b] Institute of Inorganic Chemistry, Academy of Sciences of the Czech Republic, 25068 Řež, Czech Republic
[c] J. Heyrovský Institute of Physical Chemistry, Academy of Sciences of the Czech Republic, 18223 Prague 8, Czech Republic

Another coexistence form of the three elements is silicon oxycarbide (e.g. refs.[20–23]), which is an amorphous material of the general formula SiO_xC_{4-x} and has a silica network structure in which O atoms are substituted by carbon atoms. This inorganic material shows high thermal, chemical, and mechanical stability and can be used as, for example, a catalyst support, lubricant, and in high-temperature coatings. It is also a possible candidate for anode materials of Li-ion batteries.[24] Bulky silicon oxycarbide is accessible by pyrolysis of various siloxanes,[23,24] polyphenylsilsesquioxanes,[22] or sol–gel organosilicon polymers,[20,25–28] and thin films of silicon oxycarbide were obtained by oxygen-assisted plasma CVD from polysiloxanes.[29] These represent a useful intermediate[23,25] to bulky silicon carbide. The amorphous silicon oxycarbide structures coexist with free carbon and are known as glassy blends of both constituents.

Nanosized silicon oxycarbide or silicon oxide–carbon composites have not been particularly examined so far, although nanosized H-containing Si/C/O/ (polyoxocarbosilane) phases, similar to silicon oxycarbide, were prepared by chemical vapor deposition using UV laser photolysis[30–32] and IR laser thermolysis[33–35] of disiloxanes, or by UV laser-induced conversion of silica.[36]

In the last approach, a high-fluence (MW) excimer laser irradiation of hydrocarbon (toluene) in a silica window-furnished reactor affords decomposition of hydrocarbon adjacent to the silica window, etching the silica by hot decomposition products, and deposition of fluffy nanosized composites of carbon and polyoxocarbosilane.[36]

In this paper we introduce a new, one-step approach to fabrication of nanosized and yet unknown composites of carbon and silicon oxycarbide. We show that IR laser irradiation of silica in the presence of volatile hydrocarbon (benzene or ethyne) allows deposition of thin films

of carbon–silicon oxycarbide composite and characterize these materials by spectral methods and electron microscopy.

Results and Discussion

Laser-Induced Process

The IR laser irradiation of amorphous silica in the presence of ethyne and benzene results in visible luminescence, depletion of the parent hydrocarbon, formation of volatile products, and deposition of nonadherent dark films. The depletion of benzene is somewhat slower than that of ethyne (Figure 1), which is not in line with the earlier observed higher rate of thermal decomposition of benzene compared to ethyne under conventional conditions.[37]

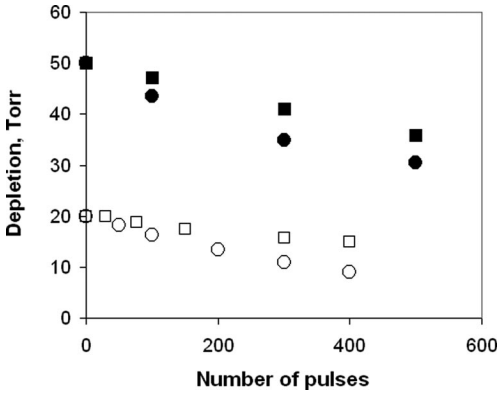

Figure 1. Depletion of benzene (squares) and ethyne (circles) as dependent on number of pulses and initial pressure (20 and 50 Torr).

The observed volatile products (Table 1) are produced via conventional thermolysis of ethyne and benzene. The prevailing ethyne and butadiyne (identified through their respective diagnostic bands at 730 and 627 cm^{-1}) formed on the irradiation in benzene are typical products of pyrolysis[38,39] and carbonization[37] of benzene and confirm that benzene is decomposed to transient C_2 and C_4 fragments. The prevailing C_3H_4 hydrocarbons (propyne:propadiene ≈ 2) and butadiyne (and other minor products) formed on the irradiation in ethyne were previously observed in conventional pyrolysis[37,40,41] and carbonization[42] of ethyne.

Carbon monoxide was observed in all experiments and its formation is explained in terms of carbothermal reduction of silica by the carbonaceous products (carbon agglomerates). These final products of the ethene and benzene decomposition are produced in copious quantities, as the volatile products are formed in much lower yields (Table 1). The efficiency of the reduction process, related to the yield of CO, is similar for carbonaceous products from benzene and ethyne. This is illustrated (Figure 2) by similar values of infrared absorbance of CO after irradiation in benzene and ethyne; $A(CO)_{benzene}/A(CO)_{ethyne}$ at 50 Torr and 500 pulses is 1.15 and that at 20 Torr and 300 pulses is 0.80.

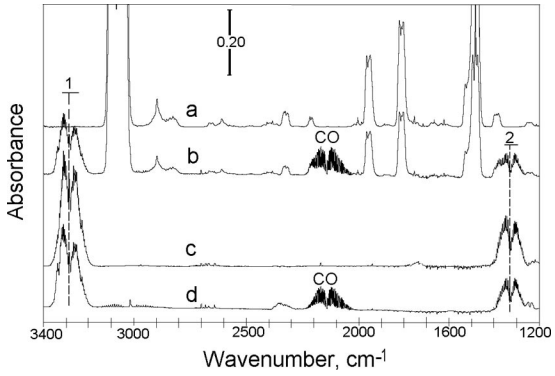

Figure 2. FTIR spectra of hydrocarbon (50 Torr) before (a, benzene; c, ethyne) and after 500 irradiation pulses (b, benzene, d, ethyne). (Bands designated as 1 and 2 correspond to ν(C–H) and combination band of C_2H_2).

Properties of Deposited Film

The coatings deposited at 20 Torr of benzene and ethyne are gray, and those deposited at the higher pressure (50 Torr) are black. They loosely adhere to the glass surface and Cu substrate. The SEM images show spongy and rather compact morphology (Figure 3) and the SEM-energy dispersive X-ray (EDX)-derived stoichiometries of several μm^2 areas (Table 2) prove (i) incorporation of silica elements in a ratio lower than in SiO_2 and (ii) the higher content of carbon in the deposits obtained at higher pressure of the hydrocarbon. The diffuse electron diffraction pattern observed for all the films is consistent with an amorphous phase in which randomly scattered crystalline nanodomains were observed by high-resolution transmission electron microscopy (Figure 4). Fourier transformation performed on these nanodomains (insets of Figure 4) confirms that the lattice image in the films from ethyne correspond[43] to orthorhombic tridymite SiO_2, (PDF 3–0227) and that in the films from benzene verifies a cubic lattice image with zone axis [220] of cristoballite (PDF 2–0278). Higher carbon

Table 1. Volatile products of benzene and ethyne decomposition.

Hydrocarbon [Torr]	No. of pulses	Dec. progress [%]	Yield of volatile products[a]	Volatile products, relative mol-%						
				CH_4	C_2H_2	C_2H_4	C_3H_4	C_3H_6	C_4H_4	C_4H_2
C_2H_2 (20)	300	45	0.01	1.6	–		49.5	6.8	3.5	38.5
C_2H_2 (50)	500	39	0.05	18.0	–		8.8	3.5	5.0	64.0
C_6H_6 (20)	400	32	0.26	0	93.0	1.0	1.0	0.1	0.9	3.6
C_6H_6 (50)	500	31	0.32	0	91.5	1.5	0.5	0.1	0.4	4.5

[a] Fraction of ethyne or benzene used for the formation of volatile products; estimated by GC analysis.

Table 2. EDX analysis of deposited films.

Hydrocarbon [Torr]	EDX-SEM stoichiometry	Selective area EDX analysis of crystalline nanodomain	amorphous region adjacent to crystalline nanodomain
C_2H_2 (20)	$Si_{1.00}O_{1.44}C_{1.13}$		
C_2H_2 (50)	$Si_{1.00}O_{1.33}C_{2.38}$	$Si_{1.00}O_{1.35}C_{2.50}$	$Si_{1.00}O_{1.13}C_{3.65}$
C_6H_6 (20)	$Si_{1.00}O_{1.60}C_{0.98}$		
C_6H_6 (50)	$Si_{1.00}O_{1.45}C_{1.76}$	$Si_{1.00}O_{1.33}C_{0.67}$	$Si_{1.00}O_{1.07}C_{0.79}$

contents in the environment of crystalline nanodomains, revealed by selective area EDX analysis (Table 2), indicates an easier crystallization of SiO_2 in C-poorer regions. The identified silica polymorphs and the fact that cristoballite occurs at temperatures (>1470 °C) higher than does tridymite suggest that temperatures of the laser process in benzene are higher than those in ethyne.

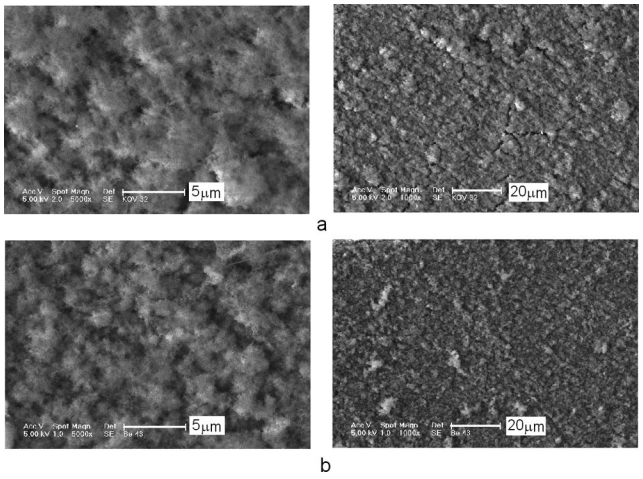

Figure 3. SEM images of the deposit obtained in ethyne (a) and benzene (b).

The FTIR spectra of the films depend little on the hydrocarbon and its pressure. Typical FTIR spectral patterns (Figure 5) are consistent[44] with intense absorption bands at 1050–1070 and 860–880 cm^{-1}, which are respectively assignable to ν_{asym}(Si–O–Si) and ν(Si–C) vibrations. A weak band at 1630 cm^{-1} and a broad band centered at ca. 3400 cm^{-1} respectively relate to ν(C=C) and ν(O–H···H) vibrational modes. The spectra do not indicate diagnostic bands of SiO_2 that are located[45] at 510 cm^{-1} [δ(OSiO)] and 1118 cm^{-1} [ν_{asym}(SiOSi)]. [The former band is missing and the latter may be hidden by the broad ν(SiOSi) band.] The spectra are thus consistent with silicon oxycarbide structures containing some unsaturated carbon and OH bonds.

The X-ray photoelectron spectra support this interpretation. The Si (2p) spectra (Figure 6) can be decomposed in two components – 102.8 ± 0.2 eV (90%) and 100.6 ± 0.2 eV (10%) for the deposit from ethyne and 103.1 ± 0.2 eV (81%) and 101.2 ± 0.2 eV (19%) for the film from benzene – which are respectively assignable[46] to $CSiO_3$ (or SiO_4) and C_3SiO structures. [The broad spectral band can be, however, compatible[46–48] with the presence of more C_nSiO_{4-n} (n = 1–3) configurations.] The C 1s spectra (Figure 7) show a peak centered at 284.8 ± 0.2 eV assignable to C–Si and C–C

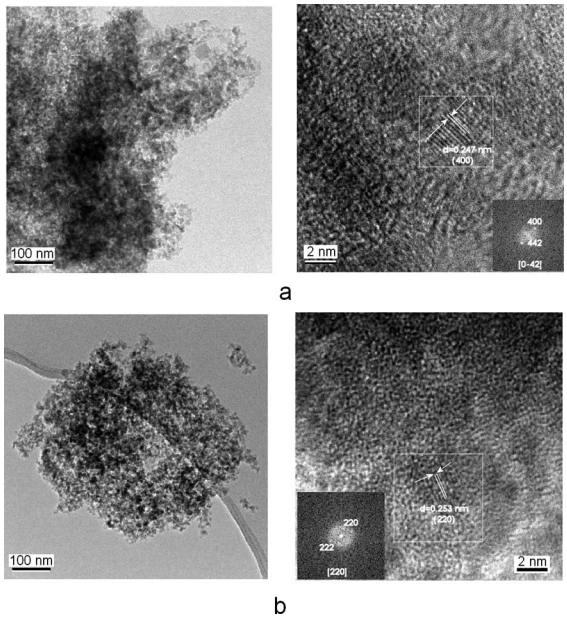

Figure 4. HRTEM images of the deposit obtained in the presence of ethyne (a) and benzene (b).

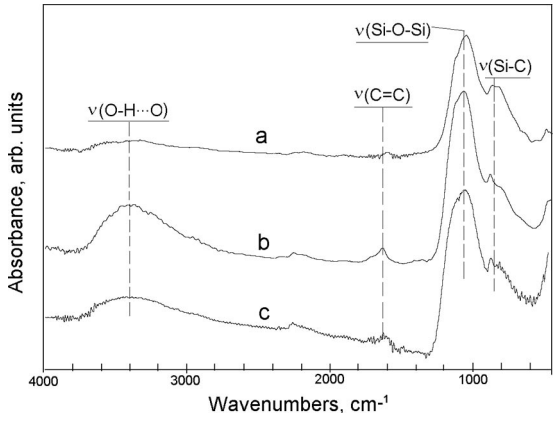

Figure 5. FTIR spectrum of the deposit obtained in ethyne (a: 50 Torr, b: 20 Torr) and benzene (c: 50 and 20 Torr).

bonds. The spectra of O 1s photoelectrons shows one peak at 533.0 ± 0.2 eV corresponding to the Si–O bond. The first derivative of the X-ray excited C KLL Auger spectra obtained from the measured samples along with the spectra taken from diamond and graphite are presented in Figure 8. An estimation[49,50] of the carbon sp^2/sp^3 hybridization ratio from the energy separation between the most positive and most negative excursions of the first derivative of the C

KLL spectra reveals that the content of sp^2 carbon in the films obtained at 50 Torr from ethyne (ca. 40%) is lower than in the film from benzene (ca. 60%).

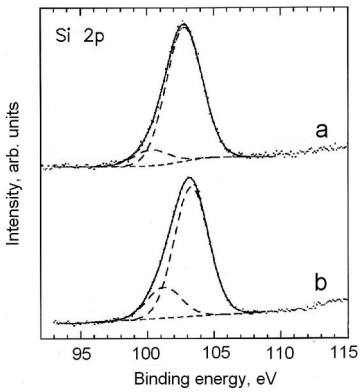

Figure 6. Si 2p core level spectra of the deposit obtained in ethyne (a) and benzene (b).

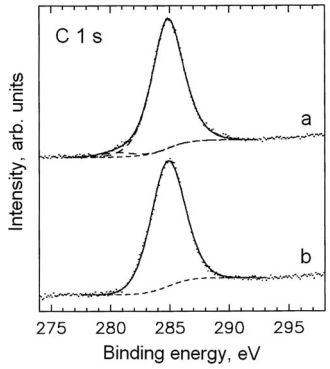

Figure 7. C 1s spectra of the deposit obtained in ethyne (a) and benzene (b).

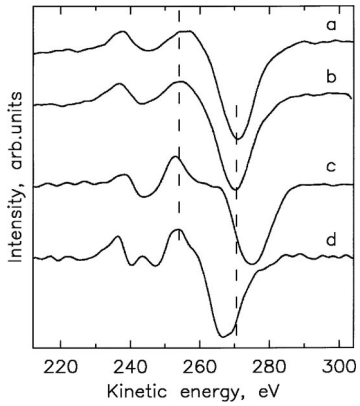

Figure 8. First derivative C KLL spectra of the deposit obtained in ethyne (a) and benzene (b) and those of graphite (c) and diamond (d).

The visible Raman spectra of the films show broad G and D bands of carbon which are respectively, centered at 1580–1600 and 1340–1370 cm^{-1}. However, the low intensity of these bands does not allow any further comment.

The above properties of the solid films are therefore consistent with amorphous carbon–silicon oxycarbide composite that incorporates nanodomains of crystalline silica. The material obtained from ethyne contains more unsaturated carbon.

Chemistry Involved

We assume that carbonaceous fragments [and their aggregates (C_nH)] produced from ethyne and benzene at the high temperatures required[37,42] react with silica in a way similar to the initial step of carbothermal reduction (SiO_2 + C(s) → SiO (g) + CO (g), ref.[7]). This reaction can occur mostly at the silica surface and to a lesser extent with SiO_2 fragments ablated from the surface. This rationale is supported by observation of silica ablation in the absence of ethyne and benzene. The gaseous SiO is a highly reactive (silylene-like[51]) species that subsequently reacts with C_nH to form the silicon oxycarbide, C_nSiO_{4-n} (n = 1–3) through addition to C=C bonds. The effective temperatures being within a few microseconds possibly above 1000 °C cause rearrangement of the initial adducts, since Si–C/Si–O scrambling occurs[23,28,52] already at around 600 °C. The complex reaction steps are briefly shown in Scheme 1.

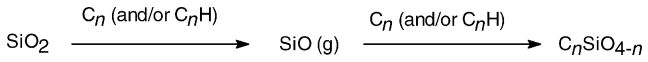

Scheme 1.

Conclusions

High infrared energy density irradiation of the silica surface in the presence of ethyne and benzene leads to carbothermal reduction of silica and results in deposition of a nanosized composite of carbon and silicon oxycarbide containing crystalline domains of silica.

The described process is the first approach to deposition of nanosized carbon–silicon oxycarbide composites and its use is suggested for production of similar nanomaterials through carbothermal reduction of other oxides.

Experimental Section

General: IR-laser irradiation experiments were conducted in a Pyrex reactor (70 mL in volume, Figure 9) containing gaseous ethyne or benzene at pressures of 20 and 50 Torr. Plates of fused silica

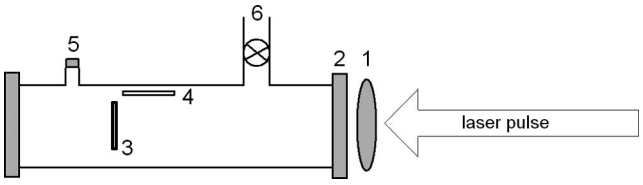

Figure 9. Vessel for irradiation of SiO_2 plate. 1: NaCl lens, 2: KBr window, 3: silica plate, 4: Cu substrate, 5: port with rubber septum, 6: valve to vacuum.

(Heraeus Quarzglas GmbH) were irradiated by a pulsed 1300 M TEA CO_2 laser (Plovdiv University) operating with a frequency of 1 Hz on the P(20) line of the 0001→1000 transition (944.19 cm^{-1}) and a pulse energy of 1.3 J. This radiation focused with a NaCl lens (incident energy density of 130 J/cm^2) was high enough to induce ablation of silica and deposition of nonadherent films on the substrate (and throughout the reactor).

The progress of ethyne and benzene decomposition and volatile decomposition products was analyzed directly in the reactor by FTIR spectrometry (the FTIR Nicolet Impact spectrometer) using diagnostic absorption bands of benzene at 1037 cm^{-1} and ethyne at 3268 cm^{-1}. Volatile products were examined directly in the reactor by FTIR spectrometry. Aliquots of the irradiated reactor content were sampled by a gas-tight syringe and analyzed by gas chromatography-mass spectroscopy (a Shimadzu QP 5050 mass spectrometer, 50-m Porabond capillary column, programmed temperature 30–200 °C). The decomposition products were identified through their FTIR spectral diagnostic bands (C_4H_2, 628 cm^{-1}; CH_4, 1305 and 3016 cm^{-1}; CO, 2175 and 2130 cm^{-1}) and through mass spectra using the NIST library. Their relative molar amounts were calculated from relative areas of GC peaks.

The films were analyzed with a FTIR Nicolet Impact spectrometer, a Nicolet Almega XR Raman spectrometer, and also by electron microscopy [a Philips XL30 CP scanning electron microscope equipped with an energy-dispersive analyzer (EDAX DX-4) of X-ray radiation and a JEOL JEM 3010 microscope operating at 300 kV and equipped with an EDS detector (INCA/Oxford) and CCD Gatan (Digital Micrograph software)]. The HRTEM analyses were carried out on ground samples that were subsequently dispersed in ethanol followed by application of a drop of the very diluted suspension on a Ni grid. The EDX atomic percentage of Si, O, and C elements was determined using a sample of poly(dimethylsiloxane) as a standard and correspond to 5% error.

The X-ray C 1s, O 1s, and Si 2p photoelectron and C KLL Auger electron spectra of the deposit were measured in an ESCA 310 (Scienta) electron spectrometer with a base pressure better than 10^{-9} Torr using Al-K_α radiation (1486.6 eV) for electron excitation. The surface composition of the deposited film was determined by correcting the spectral intensities for subshell photoionization cross sections.[53]

Acknowledgments

This work was supported by GA ASCR Grant 400720619.

[1] R. Koc, S. V. Cattamanchi, *J. Mater. Sci.* **1998**, *33*, 2537–2549.
[2] M.-J. Wang, K. Mahmud, L. J. Murphy, W. J. Patterson, *Kautsch. Gummi Kunstst.* **1998**, *51*, 348–360.
[3] Y. Mastai, S. Polarz, M. Antonietti, *Adv. Funct. Mater.* **2002**, *12*, 197–202.
[4] G. Katumba, J. Lu, L. Olumekor, G. Westin, E. Wackelgard, *J. Sol-Gel Sci. Technol.* **2005**, *36*, 33–43.
[5] D. Kawashima, T. Aihara, Y. Kobayashi, T. Koytani, A. Tomita, *Chem. Mater.* **2000**, *12*, 3397–3401.
[6] N. Klinger, E. L. Strauss, K. L. Komarek, *J. Am. Ceram. Soc.* **1966**, *49*, 369–375.
[7] C. Vix-Guterl, P. Ehrburger, *Carbon* **1997**, *35*, 1587–1592.
[8] M. L. Anderson, R. M. Stroud, D. R. Rolison, *Nano Lett.* **2002**, *2*, 235–240.
[9] Z. M. Wang, K. Hoshino, K. Shishibori, H. Kanoh, K. Ooi, *Chem. Mater.* **2003**, *15*, 2926–2935.
[10] Z. M. Wang, K. Shishibori, K. Hoshino, H. Kanoh, T. Hirotsu, *Carbon* **2006**, *44*, 2479–2488.
[11] Y. H. Chu, Z. M. Wang, M. Yamagushi, H. Kanoh, T. Hirotsu, Y. X. Zhang, *Langmuir* **2005**, *21*, 2545–2551.
[12] S. Han, T. Hyeon, *Chem. Commun.* **1999**, 1955–1956.
[13] W. Lu, E. S. Steigerwalt, J. T. Moore, L. M. Sullivan, W. E. Collins, C. M. Lukerhart, *J. Nanosci. Nanotechnol.* **2004**, *4*, 803–808.
[14] H. Müller, P. Rehak, C. Jäger, J. Hartmann, N. Meyer, S. Spange, *Adv. Mater.* **2000**, *12*, 1671–1675.
[15] V. G. Pol, S. V. Pol, P. P. George, B. Markovsky, A. Gedanken, *J. Phys. Chem. B* **2006**, *110*, 13420–13424.
[16] J. Pang, V. T. John, D. A. Loy, Z. Yang, Y. Lu, *Adv. Mater.* **2005**, *17*, 704–707.
[17] P. T. Spicer, C. Artelt, S. Sanders, S. E. Pratsinis, *J. Aerosol Sci.* **1998**, *29*, 647–659.
[18] H. K. Kammler, R. Müller, O. Senn, S. E. Pratsinis, *AIChE J.* **2001**, *47*, 1533–1543.
[19] A. Vital, J. Richter, R. Figi, O. Nagel, C. G. Aneziris, J. Bernardi, T. Graule, *Ind. Eng. Chem. Res.* **2007**, *46*, 4273–4281.
[20] E. Brewal, M. Hammond, C. G. Pantano, *J. Am. Ceram. Soc.* **1994**, *77*, 3012–3018.
[21] C. Liu, H. Zhang, S. Komarneni, C. G. Pantano, *J. Sol-Gel Sci. Technol.* **1994**, *1*, 141–151.
[22] F. I. Hurwitz, P. Heimann, S. C. Farmer, D. M. Hembreem, *J. Mater. Sci.* **1993**, *28*, 6622–6630.
[23] G. T. Burns, R. B. Taylor, Y. Xu, A. Zangvil, G. A. Zank, *Chem. Mater.* **1992**, *4*, 1313–1323.
[24] A. M. Wilson, G. Zank, K. Eguchi, W. Xing, B. Yates, J. R. Dahn, *Chem. Mater.* **1997**, *9*, 1601–1606.
[25] G. D. Sorraru, G. D'Andrea, R. Campostrini, F. Babonneau, G. Mariotto, *J. Am. Ceram. Soc.* **1995**, *78*, 379–387.
[26] G. D. Soraru, Q. Liu, L. V. Interrante, T. Apple, *Chem. Mater.* **1998**, *10*, 4047–4054.
[27] Q. Liu, W. Shi, F. Babonneau, L. V. Interrante, *Chem. Mater.* **1997**, *9*, 2434–2441.
[28] L. Bois, J. Maquet, F. Babonneau, H. Mutin, D. Bahloul, *Chem. Mater.* **1994**, *6*, 796–802.
[29] T. Fujii, T. Yokoi, M. Hiramatsu, M. Nawata, M. Hori, T. Goto, S. Hattori, *J. Vac. Sci. Technol. B* **1997**, *15*, 746–749.
[30] J. Pola, A. Ouchi, J. Šubrt, Z. Bastl, M. Sakuragi, *Chem. Vap. Depos.* **2001**, *7*, 19–22.
[31] J. Pola, A. Galíková, A. Galík, V. Blechta, Z. Bastl, J. Šubrt, A. Ouchi, *Chem. Mater.* **2002**, *14*, 144–153.
[32] J. Pola, A. Ouchi, K. Vacek, A. Galíková, V. Blechta, J. Boháček, *Solid State Sci.* **2003**, *5*, 1079–1086.
[33] Y. El Kortobi, J.-B. D'Espinose de la Cailerrie, A.-P. Legrand, X. Armand, N. Herlin, M. Cauchetier, *Chem. Mater.* **1997**, *9*, 632–639.
[34] N. Herlin-Boime, F. Ténégal, Z. Bastl, J. Šubrt, K. Jursíková, V. Blechta, J. Pola, *J. Mater. Chem.* **2002**, *12*, 1568–1572.
[35] M. Urbanová, Z. Bastl, J. Šubrt, J. Pola, *J. Mater. Chem.* **2001**, *11*, 1557–1562.
[36] J. Pola, S. Bakardjieva, M. Maryško, V. Vorlíček, J. Šubrt, Z. Bastl, A. Galíková, A. Ouchi, *J. Phys. Chem. C* **2007**, *111*, 16818–16826.
[37] R. S. Slysh, C. R. Kinney, *J. Phys. Chem.* **1961**, *65*, 1044–1045.
[38] H. J. Singh, R. D. Kern, *Comb. Flame* **1983**, *54*, 49–59.
[39] R. D. Smith, A. L. Johnson, *Comb. Flame* **1983**, *51*, 1–22.
[40] J. H. Kiefer, S. S. Sidhu, R. D. Kern, K. Xie, H. Chen, L. B. Harding, *Comb. Sci. Technol.* **1992**, *82*, 101–130.
[41] S. W. Benson, *Int. J. Chem. Kinet.* **1992**, *24*, 217–237.
[42] T. Mendiara, M. P. Domene, A. Millera, R. Bilbao, M. U. Alzueta, *J. Anal. Appl. Pyrol.* **2005**, *74*, 486–493.
[43] *JCPDS PDF-2*, release **2001**, ICDD, Newton Square, PA, USA.
[44] R. G. J. Miller, H. A. Willis (Eds.), *Infrared Structural Correlation Tables and Data Cards*, Heyden & Son Ltd., Spectrum House, London, **1969**.
[45] B. Velde, R. Couty, *J. Non-Cryst. Solids* **1987**, *94*, 238–250.

[46] C. D. Wagner in *Practical Surface Analysis* (Eds.: D. Briggs, M. Seah), *Auger and X-ray Photoelectron Spectroscopy*, vol. 1, Wiley, Chichester, UK, **1994**, p. 595.
[47] M. R. Alexander, R. D. Short, F. R. Jones, M. Stollenwerk, J. Zabold, W. Michaeli, *J. Mater. Sci.* **1996**, *31*, 1879–1885.
[48] A. Toneva, Z. Nenova, T. Marinova, V. Krastev, *Philos. Magn. A* **1997**, *75*, 331–339.
[49] A. A. Galuska, H. H. Maden, R. E. Allred, *Appl. Surf. Sci.* **1988**, *32*, 253–272.
[50] J. M. Lascovich, R. Giorgi, S. Scaglione, *Appl. Surf. Sci.* **1991**, *47*, 17–21.
[51] J. M. Jasinski, R. Becerra, R. Walsh, *Chem. Rev.* **1995**, *95*, 1203–1228.
[52] V. Belot, R. J. P. Corriu, D. Leclercq, P. H. Mutin, A. Vioux, *J. Mater. Sci. Lett.* **1990**, *9*, 1052–1054.
[53] J. H. Scofield, *J. Electron Spectrosc. Relat. Phenom.* **1976**, *8*, 129–137.

Received: May 12, 2008
Published Online: August 12, 2008

